

Baryon number segregation at the end of the cosmological quark–hadron transition

Luciano Rezzolla

International School for Advanced Studies – SISSA

Via Beirut 2–4, 34014 Trieste Italy

Physics Department, University of Illinois at Urbana-Champaign

1110 West Green St. Urbana IL 61801¹

Electronic address: rezzolla@astro.physics.uiuc.edu

Abstract

One of the most interesting questions regarding a possible first order cosmological quark–hadron phase transition concerns the final fate of the baryon number contained within the disconnected quark regions at the end of the transition. We here present a detailed investigation of the hydrodynamical evolution of an evaporating quark drop, using a multi-component fluid description to follow the mechanisms of baryon number segregation. With this approach, we are able to take account of the simultaneous effects of baryon number flux suppression at the phase interface, entropy extraction by means of particles having long mean-free-paths, and baryon number diffusion. A range of computations has been performed to investigate the permitted parameter-space and this has shown that significant baryon number concentrations, perhaps even up to densities above that of nuclear matter, represent an inevitable outcome within this scenario.

PACS number(s): 98.80.Cq, 12.38.Aw, 11.30.Fs

SISSA Ref. 144/96/A

¹Also: NCSA at the University of Illinois at Urbana-Champaign, Urbana IL 61801

I. Introduction

If the cosmological quark–hadron phase transition was of first order with non-negligible supercooling (as we will be assuming in this paper), then it almost certainly produced inhomogeneities of some kind in the spatial distribution of baryon number. These inhomogeneities could have had a relevant influence on the subsequent nucleosynthesis if they were produced on large enough scales, had sufficiently large amplitude and contained a significant fraction of the baryon number present in the Universe [1]–[7].

Many authors in the past years have calculated the possible consequences of baryon number inhomogeneities for the subsequent evolution of the Universe, focussing particularly on the scenarios for inhomogeneous nucleosynthesis [8, 9]. However, in all of these studies it was necessary to introduce suitably chosen parameters in order to compensate for lack of knowledge about the spatial distribution and amplitude of the baryon number peaks which might have been left behind at the end of the quark–hadron transition. There are various origins for this lack of knowledge which we will now discuss briefly. A first and major unresolved issue concerns the typical distance between nucleation sites at the beginning of the transition. This length scale is not only relevant at the time when hadron bubbles are nucleated within the slightly supercooled quark medium, but also represents a characteristic length scale for subsequent stages of the transition. It is the scale at which neighbouring hadron bubbles collide and percolate and it also determines the typical distance between the centres of the disconnected quark regions produced by bubble coalescence. As a consequence of this, it also represents the maximum length-scale for the production of peaks in the baryon number density at the end of the transition.

Independently of the scale over which baryon number fluctuations are produced, the study of baryon number segregation is complicated by the presence of various mechanisms which could contribute to the scale of the fluctuations. When there is chemical equilibrium between the two phases, baryon number density is already “naturally” higher in the quark phase than in the hadron phase. This difference can be further increased as a result of various other processes which probably

act together. One of these is suppression of baryon number flow across the phase interface [10, 3, 4]. Simple statistical considerations suggest that baryon number cannot be carried entirely together with the hydrodynamical flow when this moves from the quark to the hadron phase. A phenomenological explanation for this can be found in the fact that it is generally more difficult to find in a volume of 1 fm^3 and in a time of 10^{-23} sec the right triplet of up and down quarks necessary to form a color singlet nucleon (either a baryon or an antibaryon) than it is to find the doublet of quarks necessary to form the lightest hadrons (e.g. pions).

Another mechanism, which could affect the variations in baryon number density and which is effective during the final stages of the transition, is long-range energy and momentum transfer by means of particles having long mean free path (which can be viewed as a form of radiative transfer). This process, which has recently been investigated by Rezzolla and Miller [11], involves the relativistic fluids of strongly interacting particles (i.e. the hadron fluid and the quark fluid which we will refer to as “standard fluids”) and the relativistic fluid of particles having only electromagnetic and weak interactions (which we refer to as the “radiation fluid”) with entropy being extracted from the quark phase by the long mean-free-path particles of the radiation fluid. A necessary condition for this process to be significant is that the dimension R_s of the hadron phase (in the case of bubble growth) or of the quark phase (in the case of drop evaporation) needs to be roughly comparable with the smallest mean free path λ of the radiation fluid particles². When this condition is not satisfied, it is a good approximation to consider the two fluids as either being completely coupled (for $R_s \gg \lambda$) or completely decoupled (for $R_s \ll \lambda$) and the energy and momentum interchange between the standard fluid and the radiation fluid is then either maximally efficient or nonexistent.

Besides the baryon number segregating mechanisms mentioned above, there is also another competing process which needs to be taken into account. The formation

²Note that in general there are two of these length scales, referring to the electromagnetic interaction (relevant for photons, e^\pm , μ^\pm , etc., for which $\lambda \simeq 10^4 \text{ fm}$) and to the weak interaction (relevant for neutrinos and antineutrinos, for which $\lambda \simeq 10^{13} \text{ fm}$).

of localized regions of high baryon number density is counteracted by baryon number diffusion which occurs whenever a deviation from homogeneity is produced and is effective both during the quark–hadron transition and after it.

While, from the above discussion, the formation of peaks in baryon number density appears to be a rather inevitable consequence of a first order quark–hadron transition, a number of quantitative aspects of this picture still remain to be fully investigated. For this reason, and before the microphysics of baryon number flow across the phase interface or of baryon number diffusion is known in more detail, we here present results from systematic numerical computations of baryon number concentration during the evaporation of an isolated quark drop. These simulations are an extension of earlier calculations of the final stages of the quark–hadron transition, in which the hydrodynamics of a spherical isolated quark drop was coupled to the processes of relativistic radiative transfer between the standard fluids and the radiation fluid. In the present simulations, we have also studied the behaviour of the additional distinct “fluid” of baryon number carriers and have followed the progress of the segregation as it is promoted by the suppression mechanism at the interface and by the entropy extraction but moderated by baryon diffusion.

Results from computations performed with different values of the relevant parameters are presented in Section V. Before this, Section II contains a brief review of the mechanisms responsible for baryon number segregation and of their role during the various stages of the transition. Section III presents the system of relativistic equations which we use for calculating the hydrodynamics of the quark drop and the radiative transfer processes. (The formal derivation of these equations is not given here but can be found in references [12, 13, 14, 11].) In Section IV we derive a relativistic equation for the diffusion of baryon number and write it in a convenient finite difference form. This Section also introduces a phenomenological analytical expression by means of which the suppression mechanisms at the interface can be represented. Section VI contains the conclusions and also a discussion of our results in relation to the scenarios for inhomogeneous cosmological nucleosynthesis and for

the production of primordial magnetic fields. We adopt units for which $c = \hbar = k_B = 1$ and use commas or the usual “ ∂ ” notation to denote partial derivatives.

II. Evolution of the baryon number concentration

As mentioned in the Introduction, production of inhomogeneities in baryon number density can be affected by a number of different factors. In this Section we outline a schematic picture of the various stages of the transition during which baryon number segregation can either be favoured or impeded. First, we note that even in the absence of specific mechanisms for this segregation, there is a “natural” tendency for the baryon number density to be higher in the quark phase than in the hadron phase since baryon number is carried by almost massless quarks in the quark phase, whereas in the hadron phase it is carried by heavy nucleons whose number density is suppressed by an exponential factor. An estimate for the contrast in baryon number density resulting from this can easily be calculated for stages at which global chemical equilibrium is near to holding. The chemical potentials in the two phases can then be set equal ($\mu_b^q = \mu_b^h = \mu_b$) signifying that, if the phase interface were not in motion, equal fluxes of baryon number would cross it in both directions.

Because of the complexity of QCD and of the spectrum of hadronic species present in the low temperature (hadron) phase, it is necessary to make approximations if we want to obtain simple analytical expressions for the baryon number density in the two phases. Following the approach of our earlier papers, we use the phenomenological bag model for the quark phase (treating the quark-gluon plasma as consisting of relativistic non-interacting particles within a false vacuum) and the energy density and pressure may then be written as

$$e_q = g_q^* \left(\frac{\pi^2}{30} \right) T_q^4 + B, \quad p_q = g_q^* \left(\frac{\pi^2}{90} \right) T_q^4 - B, \quad (1)$$

where g_q^* is the effective number of degrees of freedom in the quark phase (including also the relevant number of degrees of freedom for the particles of the radiation fluid when the radiation and standard fluids are fully coupled [11]). The baryon number density is then given by

$$n_b^q \simeq \frac{N_c N_f}{27} \left(\frac{\mu_b}{T} \right) T^3, \quad (2)$$

where N_c and N_f are, respectively, the number of colours (three) and the number of quark flavours (which we will take here to be two). On a similar level of approximation, we can consider the pion contribution to the grand partition function of the hadron phase as being the dominant one coming from the whole spectrum of hadron species, neglect finite volume effects and the repulsive interaction between hadrons and describe the hadron phase as being essentially a gas of relativistic massless particles with the equation of state

$$e_h = g_h^* \left(\frac{\pi^2}{30} \right) T_h^4, \quad p_h = \frac{1}{3} e_h, \quad (3)$$

where g_h^* is the effective number of degrees of freedom in the hadron phase (equivalent to g_q^* in the quark phase). It is then possible to obtain a simple and compact expression for the baryon number density in the hadron phase as

$$n_b^h = \left(\frac{2mT}{\pi} \right)^{3/2} \sinh \left(\frac{\mu_b}{T} \right) e^{-m/T} \simeq \left(\frac{2mT}{\pi} \right)^{3/2} \left(\frac{\mu_b}{T} \right) e^{-m/T}, \quad (4)$$

with m being the nucleon mass.

With all of these assumptions, the contrast in baryon number density between the two phases is given by

$$R = \frac{n_b^q}{n_b^h} = \frac{N_f}{9} \left(\frac{\pi T}{2m} \right)^{3/2} e^{m/T} \sim 10 \quad \text{for } T = T_c = 150 \text{ MeV}, \quad (5)$$

where T_c is the critical temperature for the transition. Similar estimates of the baryon number contrast have been found also from more detailed analyses of the baryon number density in the two phases [15].

It is important to stress that when the hypothesis of global chemical equilibrium is valid, equation (5) holds between any two generic points in the two phases. It is reasonable to assume that global chemical equilibrium holds when the velocity of the phase interface is much smaller than the diffusion velocity of baryon number and the length scales of the disconnected hadron or quark regions are much smaller than the baryon number diffusion length-scale during the transition. This is the case, for example, soon after bubble nucleation, when most of the bubbles present have radii around the critical value

$$R_c = \frac{2\sigma}{p_h - p_q}, \quad (6)$$

where σ is the surface tension associated with the phase interface.

After nucleation, the bubble starts to expand (the low temperature phase is thermodynamically favoured) and its surface accelerates until it reaches a steady state velocity corresponding to self similar growth for a weak deflagration bubble [16]. (We are working here within the scenario of small supercooling, in which weak deflagrations are the relevant mechanism for the motion of the phase interface, and will assume that the separation between the nucleation sites is not very small.) The expansion produces a deviation away from chemical equilibrium and the baryon number density can be increased in the vicinity of the interface [4], piling up mostly on the quark side but also to some extent in the hadron phase as a result of the increased flux coming from the quark medium. The situation in the bulk of the two phases is not significantly modified, however. Diffusion tends to impede the accumulation of baryon number and, when the *self similar* growth stage is reached for the hydrodynamic variables, the baryon number density attains a *stationary* profile. (Note that the intrinsic length scale set by the diffusion coefficient prevents the baryon number density following a self similar solution.) Most of the excess

baryon number on the quark side of the interface is then within a layer of thickness r_d with the value of the baryon number density there being joined to the background value in the bulk of the quark phase via a decaying profile. A rough estimate for r_d is given by

$$r_d \approx \frac{D}{v_f}, \quad (7)$$

where D is the baryon number diffusion coefficient and v_f is the steady state velocity of the front as measured from the centre of the bubble.

The self similar growth is first broken by the coupling between the radiation fluid and the standard fluids when the bubble has reached dimensions of the order of λ [13]. After the coupling however, the similarity solution for bubble growth is restored and it ultimately ceases when the spherical compression waves preceding the deflagration fronts of neighbouring bubbles start to interact. (This occurs well before the bubble surfaces themselves come into contact.) In principle, for a perfect fluid, the compression waves would be fronted by shocks but it should be noted that the predicted amplitude of such shocks is negligibly small for the case of spherical bubbles and small supercooling which we are considering here [17, 18, 13, 19]. However, independently of whether there is any significant shock or not, the kinetic energy of the ordered motion will be progressively converted into internal energy via compression, once adjacent bubbles have started to interact, and the temperatures of both phases will be raised near to the critical temperature T_c . At this stage, the bubbles grow much more slowly, on a time scale which is essentially set by the expansion of the Universe leading to cooling which allows for continuation of the transition. In this slow growth stage, global chemical equilibrium is restored and the baryon number which has accumulated near to the phase interface can be re-distributed into the bulk of the two phases. When the surfaces of adjacent bubbles meet, they coalesce to form larger bubbles thus minimizing the total surface energy. This coalescence gives rise to disconnected quark regions which then proceed to evaporate, tending to become spherical under the action of surface tension.

The hydrodynamical evolution of isolated evaporating quark drops has been investigated in detail in a number of studies [20, 14, 11, 19] and can be essentially summarized as consisting of a self similar stage followed by one in which long range energy and momentum transfer takes place and then a final decay which may be dominated by surface tension effects and become increasingly rapid.

During the first stage, quark drops evaporate converting quarks into hadrons at the rate necessary to keep the internal compression constant and uniform. In a very pictorial description, each quark drop can be viewed as behaving like a shrinking “leaky balloon” which is ejecting material at the rate necessary to avoid producing any compression. If baryon number were entirely carried along with the hydrodynamical flow and no suppression of baryon number flux occurred at the interface, then this stage of the evaporation would not produce any increases in the baryon number density. If, however, there *is* some flux suppression, this stage will still consist of a self similar evolution for all of the hydrodynamical variables apart from the baryon number which will accumulate ahead of the interface with diffusion to either side of it in a way similar to that discussed above for a growing hadron bubble.

When the quark drop reaches dimensions comparable with the mean free path for the particles of the radiation fluid, the process of entropy extraction breaks the self similarity of the evaporation and produces a sharp increase in the fluid compression (of both the quark and hadron phases) [11] and also in the baryon number density. It should be stressed that this increase in baryon number density is distinct from the one produced by flux suppression and is not necessarily localized at the phase interface but is rather extended over the whole quark region. This is because its origin is not hydrodynamical but is the consequence of the long range energy and momentum transfer via the radiation fluid particles.

As pointed out in [14], the very final stages of the drop evaporation (for $R_s \lesssim 10^2$ fm) may be dominated by the surface tension σ which could give rise to an increasingly rapid evaporation and a consequent increase of both the compression and the baryon number density. However, recent lattice gauge calculations seem to indicate rather small values for the surface tension coefficient

$\sigma_0 = \sigma/T_c^3 \approx 0.01 - 0.02$ [18] and, if this is correct, then surface tension would play only a minor role for the increase of baryon number density.

In the next Section, we introduce the set of relativistic hydrodynamical equations which we have used for describing the dynamics of single isolated evaporating quark drops and from whose numerical solution we have derived quantitative results for the profile and amplitude of the baryon number inhomogeneity produced at the end of the quark–hadron transition.

III. Relativistic hydrodynamical equations

We here briefly review the relativistic equations which we have used for calculating baryon number concentration at the end of the quark–hadron transition and refer the reader to previous papers [12, 13, 14, 11] for further details. The equations can be divided into three main groups, related to: *i*) the dynamics of the spherical drop, *ii*) radiative transfer, *iii*) the behaviour of the diffusing “baryon number fluid”. We use a Lagrangian spherically symmetric coordinate system comoving with the fluid and having its origin at the centre of the drop. It is appropriate to write the metric line element as

$$ds^2 = -a^2 dt^2 + b^2 d\mu^2 + R^2(d\theta^2 + \sin^2\theta d\phi^2), \quad (8)$$

where μ is the comoving radial coordinate and R is the associated Eulerian coordinate. Local conservation of energy and momentum for the combined fluids (the standard fluid together with the radiation fluid), as measured in the local rest frames of the standard fluid, can be expressed as the vanishing of the projections of the combined stress-energy tensor parallel and perpendicular to the direction of the fluid four-velocity \mathbf{u} . Using this, the continuity equation and the Einstein equations, the full set of equations for determining the behaviour of the standard fluids can be written as:

$$u_{,t} = -a \left[\frac{\Gamma}{b} \left(\frac{p_{,\mu} + bs_1}{e + p} \right) + 4\pi GR \left(p + \frac{1}{3}w_0 + w_2 \right) + \frac{GM}{R^2} \right], \quad (9)$$

$$e_{,t} = w\rho_{,t} - as_0, \quad (10)$$

$$\frac{(\rho R^2)_{,t}}{\rho R^2} = -a \left(\frac{u_{,\mu} - 4\pi GbRw_1}{R_{,\mu}} \right), \quad (11)$$

$$\frac{(aw)_{,\mu}}{aw} = -\frac{w\rho_{,\mu} - e_{,\mu} + bs_1}{\rho w}, \quad (12)$$

$$M_{,\mu} = 4\pi R^2 R_{,\mu} \left(e + w_0 + \frac{u}{\Gamma} w_1 \right), \quad (13)$$

$$b = \frac{1}{4\pi R^2 \rho}, \quad u = \frac{1}{a} R_{,t}, \quad (14)$$

$$\Gamma = \frac{1}{b} R_{,\mu} = \left(1 + u^2 - \frac{2GM}{R} \right)^{1/2}, \quad (15)$$

where $w = (e + p)/\rho$ is the specific enthalpy of the standard fluids, u is the radial component of the fluid four velocity in the associated Eulerian frame, Γ is the general relativistic analogue of the Lorentz factor and M a generalized mass function. The quantity ρ is the compression factor which expresses the variation in proper volume of comoving elements of the standard fluids with respect to a fiducial value. (For a classical standard fluid, ρ can be taken to represent the rest mass density). The interaction between the standard fluids and the radiation fluid enters through the source functions s_0 and s_1 and through the radiation contributions to the gravitational terms via the radiation energy density w_0 , energy flux w_1 and anisotropy w_2 . The latter quantities are calculated by considering local conservation of energy and momentum of the radiation fluid alone, and this provides the following set of equations [12]

$$(w_0)_{,t} + \frac{a}{b}(w_1)_{,\mu} + \frac{4}{3}\left(\frac{b_{,t}}{b} + \frac{2R_{,t}}{R}\right)w_0 + \frac{2a}{b}\left(\frac{a_{,\mu}}{a} + \frac{R_{,\mu}}{R}\right)w_1 + \left(\frac{b_{,t}}{b} - \frac{R_{,t}}{R}\right)w_2 = as_0, \quad (16)$$

$$(w_1)_{,t} + \frac{a}{b}\left(\frac{1}{3}w_0 + w_2\right)_{,\mu} + \frac{4a_{,\mu}}{3b}w_0 + 2\left(\frac{b_{,t}}{b} + \frac{R_{,t}}{R}\right)w_1 + \frac{a}{b}\left(\frac{a_{,\mu}}{a} + \frac{3R_{,\mu}}{R}\right)w_2 = as_1, \quad (17)$$

$$w_2 = f_E w_0, \quad (18)$$

where (18) is a closure relation written in terms of a variable Eddington factor f_E .

In our calculations, the source functions s_0 , s_1 are expressed as

$$s_0 = \frac{(1 + \alpha_2)}{\lambda} \left[g_r \left(\frac{\pi^2}{30} \right) T_F^4 - w_0 \right], \quad s_1 = -\frac{w_1}{\lambda}, \quad (19)$$

with g_r and T_F being the number of degrees of freedom and the temperature of the radiation fluid. The parameter α_2 is an adjustable coefficient (ranging between zero and one) which takes account of the contribution of non-conservative scatterings to the energy source function (for the present calculations we take $\alpha_2 = 1$). We treat the phase interface as a discontinuity surface and track it continuously through the finite difference grid using junction conditions which are imposed across the interface and a characteristic form of the above hydrodynamic equations which is used for the flow regions adjacent to it. A detailed discussion of these extra equations and of the way in which they are obtained has been given in previous papers [12, 13, 11] and we will not repeat it here but, rather, just list the expressions used for the junction conditions. The energy and momentum junction conditions for the standard fluids are expressed as

$$[(e + p)ab]^\pm = 0, \quad (20)$$

$$[eb^2\dot{\mu}_s^2 + pa^2]^\pm = -\frac{\sigma f^2}{2} \left\{ \frac{1}{ab} \frac{d}{dt} \left(\frac{b^2\dot{\mu}_s}{f} \right) + \frac{f, \mu}{ab} + \frac{2}{fR} (b\dot{\mu}_s u + a\Gamma) \right\}^\pm. \quad (21)$$

As junction conditions for the energy and momentum of the radiation fluid after the decoupling from the standard fluids has begun to take place [11] we use:

$$\left[ab\dot{\mu}_s \left(\frac{4}{3} + f_E \right) w_0 - (a^2 + b^2\dot{\mu}_s^2) w_1 \right]^\pm = 0, \quad (22)$$

$$\left[\left\{ a^2 \left(\frac{1}{3} + f_E \right) + b^2\dot{\mu}_s^2 \right\} w_0 - 2ab\dot{\mu}_s w_1 \right]^\pm = 0, \quad (23)$$

while for the metric coefficients we have:

$$[R]^\pm = 0, \quad (24)$$

$$[au + b\dot{\mu}_s\Gamma]^\pm = 0, \quad (25)$$

$$[a^2 - b^2\dot{\mu}_s^2]^\pm = 0. \quad (26)$$

Note that the use of brackets in equations (20)–(26) follows the conventions: $[A]^\pm = A^+ - A^-$, $\{A\}^\pm = A^+ + A^-$, and that the superscripts $^\pm$ indicate quantities immediately ahead of and behind the interface. The interface location is denoted by μ_s with $\dot{\mu}_s = d\mu_s/dt$ and $f = (a^2 - b^2\dot{\mu}_s^2)^{1/2}$.

Finally, for a phase interface which behaves as a weak deflagration front, it is necessary to supply one further equation giving the rate at which material is converted from one phase to the other (or, alternatively, to specify the interface velocity). As discussed in previous papers (see, for example [16]) we use a formula giving the rate of conversion of quarks into hadrons in terms of a black-body model

for the phase interface, suitably corrected with an adjustable accommodation coefficient α_1 ($0 \leq \alpha_1 \leq 1$) to take account of deviations away from an ideal black-body law. We then have

$$-\frac{aw\dot{\mu}_s}{4\pi R_s^2(a^2 - b^2\dot{\mu}_s^2)} = \left(\frac{\alpha_1}{4}\right)(g_h + g_r) \left(\frac{\pi^2}{30}\right)(T_q^4 - T_h^4). \quad (27)$$

For the calculations presented here, we have taken $\alpha_1 = 1$, but an extend discussion of computations with smaller values of $\alpha_1 = 1$ can be found in [11].

IV. Baryon number flux and diffusion

As mentioned in the Introduction, simple considerations seem to suggest that baryon number would not be carried along entirely together with the hydrodynamical flow but, rather, that it would tend to be “trapped” inside the high temperature phase because of flux suppression at the phase interface. In order to study the evolution of the baryon number distribution, we need to extend the multi-component fluid description discussed in Section III by adding to the treatment of the standard fluids and the radiation fluid, an additional “baryon number fluid”. In particular, we need to introduce equations to describe the hydrodynamics of a fluid which has a suppressed flow at the phase interface and which diffuses relative to the standard fluids.

The effects of this diffusion can be included by introducing a diffusive flux four-vector \mathbf{q} into the baryon number continuity equation which becomes

$$(n_b u^\alpha + q^\alpha)_{;\alpha} = 0, \quad (28)$$

where n_b is the baryon number density, \mathbf{u} is still the four velocity of the *standard* fluid and Greek indices are taken to run from 0 to 3. In the frame comoving with the standard fluid, $u^\alpha \equiv (1/a, 0, 0, 0)$ and \mathbf{q} has only a spatial component [i.e.

$u_\alpha q^\alpha = 0$ and $q^\alpha \equiv (0, q^\mu, 0, 0)$. Using the property $(V^\alpha)_{;\alpha} = (\sqrt{-g}V^\alpha)_{;\alpha}/\sqrt{-g}$ (where g is the determinant of the metric tensor) and the metric relations (8), (15), we can rewrite (28) as

$$bR^2 \left[\frac{\partial(n_b)}{\partial t} + \left(\frac{an_b}{R^2} \right) \frac{\partial(uR^2)}{\partial R} \right] = \frac{aR^2}{\Gamma} \frac{\partial(b\Gamma)}{\partial R} \frac{\partial(Dn_b)}{\partial R} + ab^2\Gamma \frac{\partial}{\partial R} \left[\frac{R^2}{b\Gamma} \frac{\partial(Dn_b)}{\partial R} \right], \quad (29)$$

(see the Appendix for details) where the radial component of the diffusive flux is written as

$$q^\mu \equiv -\frac{1}{(b\Gamma)^2} \frac{\partial(Dn_b)}{\partial \mu} = -\frac{1}{b\Gamma} \frac{\partial(Dn_b)}{\partial R}. \quad (30)$$

In the Newtonian limit, $\Gamma = a = 1$ and equation (29) reduces to the standard Lagrangian diffusion equation in spherical coordinates, with D being the diffusion coefficient (note that here, $\partial/\partial t$ is a Lagrangian time derivative for a location comoving with the standard fluid). An attractive feature of Lagrangian schemes is that advection is treated exactly. Exploiting this, it is convenient to use for the finite-difference representation of equation (29), the simple and compact expression:

$$\begin{aligned} 4\pi(n_b)_{j+1/2}^{n+1} \left[\frac{(R^2)_{j+1/2}^{n+1}}{\Gamma_{j+1/2}^{n+1}} \right] \Delta R_{j+1/2}^{n+1} &= 4\pi(n_b)_{j+1/2}^n \left[\frac{(R^2)_{j+1/2}^n}{\Gamma_{j+1/2}^n} \right] \Delta R_{j+1/2}^n \\ &\quad - \frac{4\pi}{\Gamma_{j+1/2}^{n+1/2}} \left[(R^2)_{j+1}^n (\Phi_D)_{j+1}^n - (R^2)_j^n (\Phi_D)_j^n \right] a_{j+1/2}^{n+1/2} \Delta t_{j+1/2}^{n+1/2}, \end{aligned} \quad (31)$$

where the superscripts refer to the time level at which the quantity is calculated and the subscripts to the position in the spatial grid, $\Delta R_{j+1/2}^n = R_{j+1}^n - R_j^n$ and

$$(\Phi_D)_j^n = -D \left[\frac{(n_b)_{j+1/2}^n - (n_b)_{j-1/2}^n}{R_{j+1/2}^n - R_{j-1/2}^n} \right], \quad (32)$$

is the diffusive flux of baryon number. A rough estimate for the value of the diffusion coefficient D (which we take to be constant in time, uniform in space and the same in both phases) can be deduced with rather simple arguments if we rule out the possibility of the diffusion being turbulent [5] (which seems likely to be correct [9]). In this case, baryon number diffusion can be described as a simple Brownian motion of baryon number carriers having a mean free path of the order $\lambda_{free} \gtrsim T_c^{-1}$ [4] giving a microscopic diffusion coefficient $D \sim 10^{-1} - 10$ fm.

Clearly, the baryon number within a given grid zone changes in time only if a baryon flux crosses its boundaries. While for the bulk of the two phases, the flux leading to the variation is just the diffusive flux (32), a special treatment is necessary for the two parts of the grid zone containing the phase interface. At the interface, the diffusive flux is accompanied by a much larger flux which is related to the hydrodynamical flow Φ_ρ of elements of the quark gluon plasma as it is converted to the hadron phase. As mentioned earlier, this flux could be subject to suppression processes at the interface but no exact expression is yet available for this. We therefore proceed here by defining a phenomenological expression for the net baryon number flux across the interface Φ_b in terms of the hydrodynamical flux Φ_ρ and a suitable “filter factor” F which expresses the ratio between the baryon number passing across the phase interface and the total baryon number incident on it.

In principle, F could be expressed in terms of the probability of finding (from all of the quarks and antiquarks present) three quarks of the right types within a volume of 1 fm^3 and in a time of 10^{-23} s, in terms of the “transparency” of the phase interface to the passage of a baryon number carrier from the quark phase to the hadron phase $\Sigma_{q \rightarrow h}$ and of the corresponding probability $\Sigma_{h \rightarrow q}$ that a baryon hitting the phase boundary from the hadron phase is absorbed [3]. Moreover, referring to a situation in which chemical equilibrium holds, it would be possible to express $\Sigma_{q \rightarrow h}$ in terms of $\Sigma_{h \rightarrow q}$ and this would restrict the uncertainty to this latter quantity only. (Although convenient, this approach requires that the baryon transmission probability does not vary significantly when the equilibrium is broken.)

Unfortunately, no reliable value for the baryon transmission probability $\Sigma_{h \rightarrow q}$ is known at present and, worse than this, different approaches to the study of the rates of elementary processes taking place at the phase interface seem to result in quite different estimates of it (see [3, 21] and [6] for further references). In view of this uncertainty, we will treat the filter factor as essentially a free parameter, adopting the reference value $F \sim 10^{-1}$ as estimated from the expressions presented by Fuller et al. [3] for $T_c = 150$ MeV and $\Sigma_{h \rightarrow q} \sim 10^{-3}$. (The value $F = 1$ corresponds to the case where the baryon number flow crosses the phase interface unimpeded and clearly represents an upper limit.)

The flux of elements of the standard fluid across the interface can be evaluated by projecting the flux four-vector along the unit spacelike four-vector \mathbf{n} normal to the timelike hypersurface describing the time evolution of the interface. We obtain

$$\Phi_\rho \equiv \rho u^\alpha n_\alpha = -\frac{\dot{\mu}_s}{4\pi R_s^2 f}, \quad (33)$$

where $\dot{\mu}_s < 0$, $f = (a^2 - b^2 \dot{\mu}_s^2)^{1/2}$ and

$$u^\alpha \equiv \frac{1}{a}(1, 0, 0, 0), \quad n_\alpha \equiv \frac{ab}{f}(-\dot{\mu}_s, 1, 0, 0). \quad (34)$$

Neglecting diffusive contributions to the baryon number flux across the interface, we obtain

$$\Phi_b = F \left(\frac{n_b^q}{\rho_q} \right) \Phi_\rho = -F \left(\frac{n_b^q}{\rho_q} \right) \left(\frac{\dot{\mu}_s}{4\pi R_s^2 f} \right), \quad (35)$$

and we assume continuity of this flux across the interface (i.e. $[\Phi_b]^\pm = 0$).

In the next Section we will present results from numerical computations made using the set of equations which we have introduced here and illustrate the roles played in the segregation of baryon number by suppression mechanisms and by radiative transfer.

V. Numerical strategy and results

The numerical approach implemented for the solution of the present set of equations (9)–(15), (16)–(19), (20)–(26) and (29) is based on that used for our earlier computation of the evaporation of a quark drop including the effects of long range energy and momentum transfer [11] with an extension to include the parabolic diffusion equation (29).

As is frequently the case for numerical computations in which a diffusion equation needs to be solved, we are here faced with the problem of performing calculations with a mixed set of equations and avoiding excessive restrictions placed on the time step by the von Neumann criterion for stability in solving the parabolic equation. Obeying this criterion, which is more stringent than the usual Courant one since it depends quadratically on the minimum grid spacing and is inversely proportional to the diffusion coefficient [22], allows one to perform an explicit integration of equation (31) without any further constraint. However, for the present case, implementing the von Neumann condition produced computational times for each simulation which were not affordable. The reason for this is connected with the particular organization of our grid which has an exponentially increasing spacing in order to facilitate following the dynamics of the drop through several orders of magnitude change in the radius. To avoid this problem, we have implemented a standard “flux limiter” scheme in which a control is set on the diffusive flux in the quark phase preventing it from evacuating the baryon number content of any grid zone within a single time-step [23]. The results obtained in this way were found to be in excellent agreement with ones from a comparison calculation without the flux limiter and using the von Neumann condition (but which required a computational time longer by a factor of twenty).

Another concern in the present calculations has been that of preserving as closely as possible the overall conservation of baryon number. Clearly results for the final distribution of baryon number at the end of the transition will be worthless if the integration of the diffusion equation (31) is not accurate enough and is significantly

producing or destroying baryon number. This equation is nearly conservative in form but special attention needed to be paid to the calculation of interpolated values for a and Γ (for which we used function fitting procedures) and to the implementation of the regridding procedure [14, 11]. Having done this, our computations preserve the total baryon number in the grid to an accuracy of a few parts in 10^8 for runs of about 10^6 time steps.

In the following, we present results from computations which have been performed evolving from initial data given by the self similar solutions derived in [14] for a spherical quark drop with initial dimensions $R_{s,0} = 10^7$ fm, at an initial temperature $\hat{T}_q = T_q/T_c = 0.998$, surrounded by a hadron plasma at temperature $\hat{T}_h = T_h/T_c = 0.990$. The similarity solutions provide suitable initial conditions for all of the variables apart from the baryon number which does not necessarily follow the bulk hydrodynamical flow. We decided to start with the baryon number density in each phase being uniform and given by the expressions (2) and (4) presented in Section II which correspond to conditions of chemical equilibrium. This is very approximate because global chemical equilibrium does not apply for a situation with a moving interface such as the one which we are considering but, nevertheless, initial conditions imposed in this way are sufficiently good to allow the solution to relax rapidly to a consistent one.

We have examined the effects on the overall solution of varying the values of important input parameters and we will be discussing this in detail but first we concentrate on the results obtained for a set of fiducial parameter values. This “standard” run follows the evaporation of a quark drop with surface tension parameter $\sigma_0 = 0.01$, filter factor $F = 0.3$ and diffusion coefficient $D = 1$ fm. The decoupling radius R_d (i.e. the drop radius at which the decoupling between the standard fluids and the radiation fluid is allowed to take place [11]) is set to be 10^4 fm, which corresponds to the average mean free path of the electromagnetically-interacting particles. We do not consider here a decoupling with neutrinos which, however, would follow a similar hydrodynamical behaviour except for the different number of degrees of freedom involved [11].

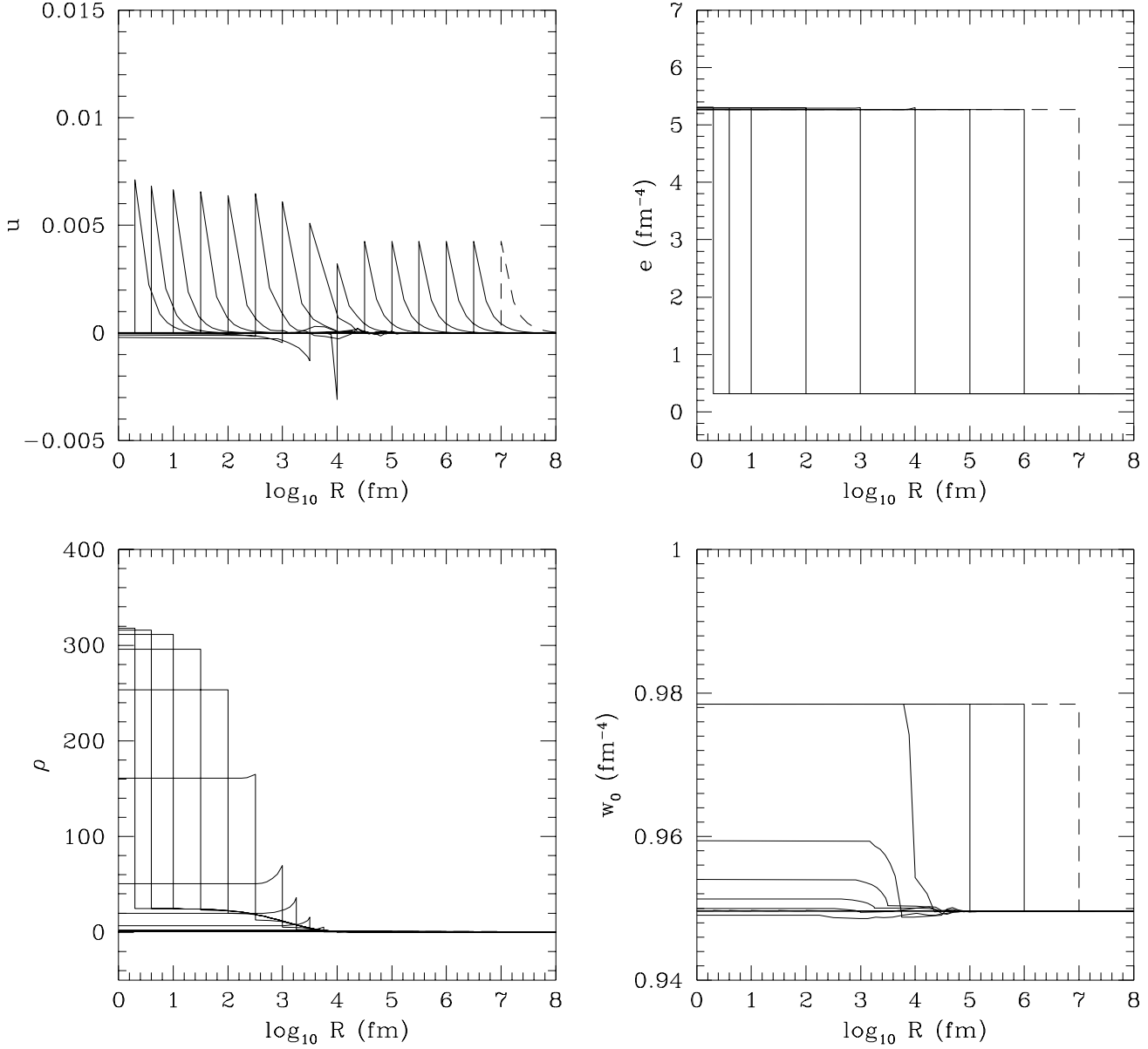


Figure 1. Time evolution of the most significant hydrodynamical variables. Each curve refers to a given time in the solution, with the quark phase being to the left of the vertical discontinuity and the initial conditions being indicated with the dashed curves. Starting from the upper left-hand window and proceeding clockwise, the frames show: the radial component of the fluid four-velocity in the Eulerian frame u , the energy densities of the standard fluids e and of the radiation fluid w_0 and the compression factor ρ . The decoupling between the radiation fluid and the standard fluids is allowed to start at $R_s = 10^4$ fm

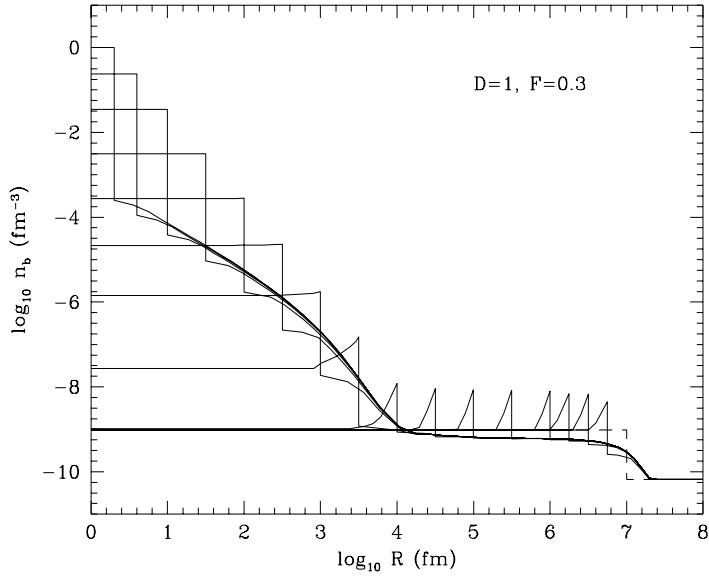


Figure 2. Time evolution of the logarithm of the baryon number density. The continuous curves refer to successive stages in the evolution, with the initial conditions being indicated by the dashed curve.

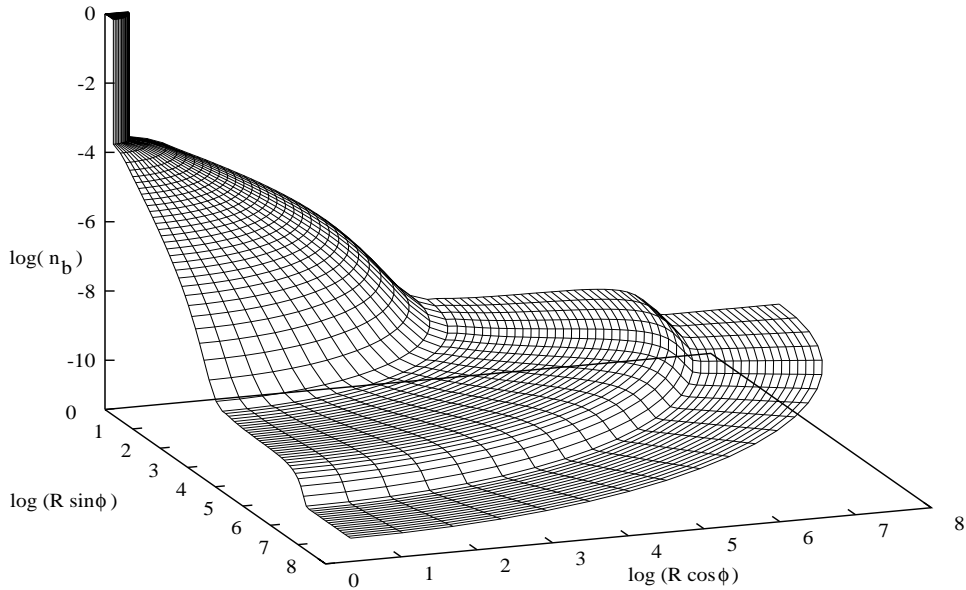


Figure 3. Three-dimensional plot of the profile of the log of the baryon number density at the end of the computation, when the quark drop had a radius $R_s = 2$ fm.

This decoupling would take place at a scale $\lambda_\nu \simeq 10^{13}$ fm but it is not currently clear whether spherically isolated quark drops would have been present at that scale.

Figure 1 shows the time evolution of the most important hydrodynamical variables: the radial component of the fluid four-velocity u , the energy density of the standard fluids e , the compression factor ρ and the energy density of the radiation fluid w_0 . Although similar curves have already been presented and discussed in [11], we consider it useful to show them here as they provide the hydrodynamical background for our discussion of baryon number segregation.

The main features of the hydrodynamical solution can be summarized as follows: *i)* the presence of a self similar solution until the radiation decoupling starts at $R_s = R_d$; *ii)* the recovering of an “almost” self similar solution for the energy density e and the fluid velocity u after decoupling; *iii)* the significant increase of the compression factor in both phases caused by the extraction of entropy by the radiation fluid; *iv)* the smoothing out of the step in the profile of the radiation energy density when decoupling occurs.

In Figure 2 we show the time evolution of the baryon number density which, for convenience, we can divide into three main stages. In the first of these, baryon number density deviates from the imposed initial conditions and settles into a solution which is consistent with the motion of the interface. As mentioned above, the initial conditions adopted assume chemical equilibrium to hold across the phase interface. However, when the interface is in motion (as it is for our initial conditions), equilibrium cannot hold and the baryon number density in the hadron phase has to adjust itself in order to reach a self consistent solution. By the time the drop radius has decreased from 10^7 fm to approximately 2.5×10^6 fm, the new solution has reached its steady state configuration.

The next stage of the evolution is characterized by a “snowplow” behaviour of the phase interface which accumulates baryon number as it moves into the quark medium. This piling-up of baryon number on the quark side is counteracted by the effects of diffusion which tends to smear out the build-up, producing a rapidly decaying profile (a similar behaviour was also suggested by Kurki-Suonio [4]). During this stage, which corresponds to a self similar solution for the hydrodynamical variables

presented in Fig. 1, the counteracting mechanisms of baryon number flux suppression and of baryon diffusion, suitably regulate the rate of baryon number passage across the phase interface until a stationary solution is reached for the baryon number density. Note that the length scale r_d is too small to be resolved on the grid at this stage and this explains why, in Fig. 2, the decaying profile appears to have a constant logarithmic width (connected with the grid structure).

The self similar solution for the hydrodynamical variables can be maintained only as long as the quark drop evaporation is effectively scale free and no other process is intervening. Equivalently, the stationary solution for baryon number can be maintained only as long as the underlying hydrodynamical behaviour remains self similar and the tail of the diffusing profile does not interact with the centre of the drop (the time when this happens is dependent on the magnitude of D). In the present situation there are two possible length scales that when reached by the drop radius would produce a deviation away from the hydrodynamic similarity solution. These are the mean free path of the radiation fluid particles (at which scale the radiative transfer is most effective) and the length scale set by the surface tension (which is much smaller).

For our fiducial parameter values, the radiative transfer occurs before the drop can know about its centre via diffusion and, as a consequence, the following stage of the evolution in Fig. 2 starts at $R_s = 10^4$ fm. When we compare the effects of the entropy extraction via radiative transfer on the compression factor (lower-right window in Fig. 1) and on the baryon number density, we can find analogies and differences. The first common feature is the increase of ρ (and of n_b) *also* in the low temperature phase for $R_s < 10^4$ fm. However, while the radius at which the compression increase in the hadron phase begins does not change in time, this is not the case for the radius at which the increase in baryon number density begins. The latter slowly shifts towards larger values under the action of baryon diffusion.

Figure 3 shows a three-dimensional representation of the profile of baryon number density at the end of the computation when the quark drop has radius $R_s = 2$ fm.³

Another difference between the evolution of the compression factor and that of the baryon number density is the larger increase in the latter (about 9 orders of magnitude) produced after radiation decoupling. This is due to the fact that baryon number density can be increased not only by the entropy extraction via radiative transfer but also by flux suppression at the interface and the latter is a much more effective mechanism. Note that the profile of baryon number density shown in Fig. 3 corresponds to material which has non-uniform specific entropy (as a result of radiative transfer [11]), but which is very nearly in thermal and mechanical equilibrium in each phase [9, 10].

When looking at the profiles in Figures 2 and 3 it is not possible to distinguish the different contributions coming from the radiative transfer and from the flux suppression. However, using the mean free path of the radiation particles λ as a free parameter, it is possible to regulate the action of the radiative transfer. Taking $\lambda = 0$ corresponds to a situation in which the decoupling never takes place at all. Figure 4 shows the final profile of the baryon number density when the quark drop has radius $R_s = 2$ fm as calculated for progressively smaller values of the mean free path, which is equal to $\lambda = 10^4$ fm for the heavy continuous curve, $\lambda = 10^2$ fm for the dashed curve and to zero for the dotted one.

The effects of radiative transfer can be clearly seen by comparing the dotted curve with the heavy continuous curve and amount to a relative increase in the baryon number density of around one order of magnitude in the inner part of the profile. Note that the use of a logarithmic scale can be misleading and seem to suggest that total baryon number in the different plots is not the same. However, when comparing profiles for different values of λ , one should pay particular attention to differences in the outer regions which are not very noticeable but which make a

³It is important to stress that, we here stop our computations at $R_s = 2$ fm because already at this stage the whole hydrodynamical approach described in Sections I–III is ceasing to be valid. It is no longer sensible to use a *fluid* description for a quark drop containing only very few quarks.

considerable contribution. In order to emphasize these differences, a magnification of the final profiles is shown in the small diagram at the top right of Figure 4.

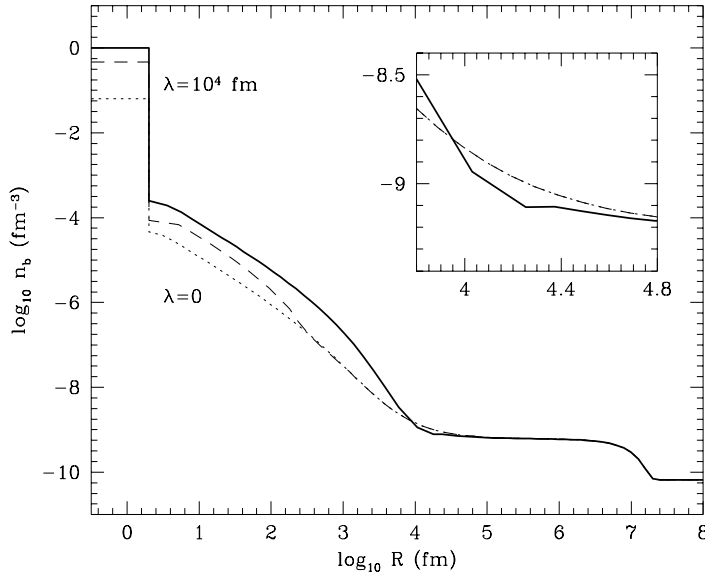


Figure 4. Final profile of the baryon number density when the quark drop has radius $R_s = 2$ fm as calculated for different values of the mean free path λ . The curves correspond to $\lambda = 10^4$ fm (heavy continuous curve), 10^2 fm (dashed curve) and 0 (dotted curve). The small diagram at the top right shows a magnification of the differences between the curves.

Figure 5 shows results from calculations performed with different values of the filter factor, showing the final profiles of baryon number density when the drop has radius 2 fm. Different curves refer to values of the filter factor F ranging from 0.2 to 1, with the heavy continuous curve corresponding to the preferred value $F = 0.3$.

The behaviour of the solution under variation of the filter factor F is straightforward to understand: a *more* “transparent” phase interface (i.e. with a higher value of F) leads to less accumulation of baryon number inside the drop and produces a smaller final increase in the baryon number density. However, because of

the nonlinearity of the process, a *less* transparent interface actually gives a larger net baryon number flux as a consequence of the increased baryon number density in the quark phase [see equation (35)]. This explains why the baryon number density is larger also outside the quark drop. Note that also in this figure, the logarithmic scaling could be confusing and suggest that the total baryon number is not the same for the different curves. However, once again, as shown in the small magnified diagram, the large differences which appear for $R_s < 10^4$ fm are compensated by changes further out which are less easy to see.

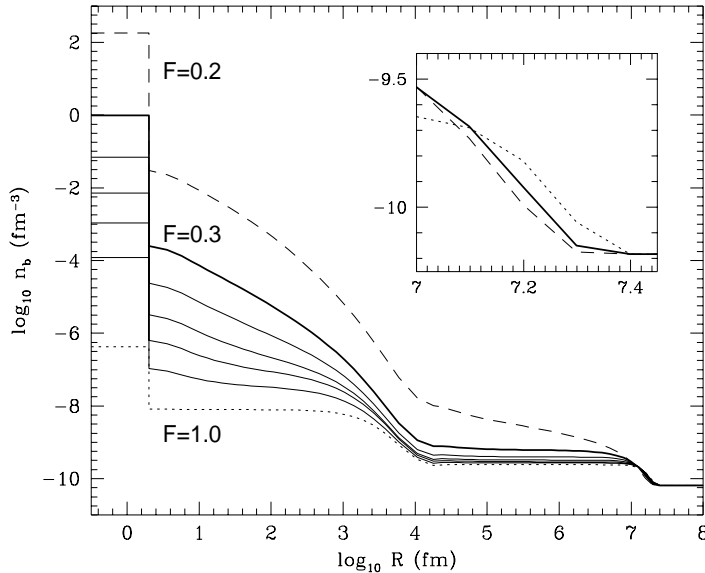


Figure 5. Final profile of the baryon number density when the quark drop has radius $R_s = 2$ fm as calculated for different values of the filter factor at the interface F . The curves correspond to $F = 0.2$ (dashed curve), $F = 0.3$ (heavy continuous curve), $F = 0.4, 0.5, 0.6, 0.7$ (standard continuous curves) and $F = 1$ (dotted curve). The small diagram at the top right shows a magnification of the differences between the most important curves.

A number of comments should be made about the final baryon number density reached inside the quark phase for different values of the filter factor. As shown by

the curve corresponding to $F = 0.2$, the baryon number density in the quark phase could well reach values above that for nuclear matter and this could suggest that a transition to strange quark nuggets might possibly occur at some stage during the quark drop evaporation. This is a very speculative idea and we limit ourselves to pointing out that, as far as baryon number segregation is concerned, conditions for the creation of quark nuggets are not difficult to reach if a strong suppression of baryon number flux takes place at the interface. Another important point to notice is that with the present choice of parameter values, only a very small fraction of the initial total baryon number will remain in the high density regions after drops have evaporated away. A final comment should be made about the properties of the final baryon number density profile obtained for $F = 1$, which corresponds to a situation in which baryon number carriers are freely streaming across the interface and is the result of radiation decoupling only. Although this case may well not refer to a realistic scenario, it is instructive as it shows the role of the baryon flux suppression in the production of baryon number density peaks. It is interesting to compare this with the $\lambda = 0$ curve of Fig. 4 which corresponds to radiative transfer not being operative.

We conclude our analysis of the numerical results by presenting the final baryon number density profiles obtained after varying the diffusion coefficient while maintaining the other parameters with their standard values. Figure 6 shows curves calculated for values of D ranging between zero (dotted curve) and 10 and with the heavy continuous curve corresponding to the preferred value $D = 1$.

The curves demonstrate the action of diffusion which prevents the accumulation of baryon number in a narrow shell ahead of the phase interface (as seen for $D = 0$) and spreads out the accumulation of baryon number produced in the hadron phase near to the drop surface. Larger values of the diffusion coefficient give rise to larger final values of the baryon number density in the quark phase, but the results show that the high number density regions are unlikely to contain a large fraction of the total baryon number if only microscopic random diffusion is taken into account (which leads to relatively small values for D).

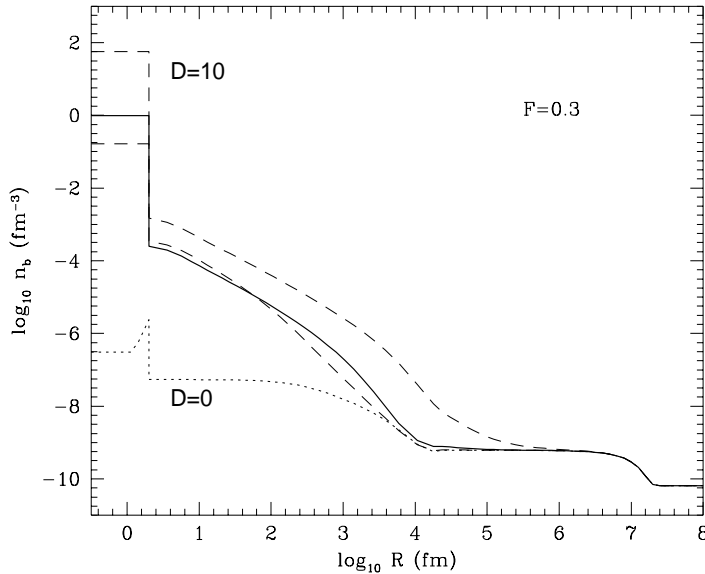


Figure 6. Final profile of the baryon number density when the quark drop has radius $R_s = 2$ fm as calculated for different values of the diffusion coefficient D . The curves correspond to $D = 10$, 1 (the heavy continuous line), 0.1 and 0 (the dotted curve).

Stronger diffusion is more efficient in preventing accumulation of baryon number adjacent to the quark side of the interface and this, in turn, tends to reduce the outward flux of baryon number into the hadron phase. The effective role played by diffusion is then that of trapping baryon number within the high density region and so it is no surprise that higher final values of n_b should result for larger values of D . It is worth underlining that the values adopted for our simulations refer to a microscopic modeling of diffusive processes in which turbulent motion is neglected. It is possible that non radial fluid motions could produce a larger effective diffusion coefficient, but not enough is yet known about this.

VI. Conclusions

We have presented here results from numerical computations of the final stages of a first order cosmological quark–hadron phase transition, aiming to estimate the baryon number density profile produced. For doing this, we have used mathematical and numerical techniques previously developed for following the evaporation of spherical quark drops together with a separate treatment of a distinct fluid of baryon number carriers. The effects of baryon number flux suppression at the phase interface and of baryon number diffusion have been included within the overall relativistic hydrodynamical treatment. The results obtained have shown that baryon number segregation is an inevitable result of a first order transition and illustrate the different roles played in baryon number segregation by flux suppression and by radiative transfer. Final baryon number density profiles have been computed which exhibit relative increases of several orders of magnitude in both phases, with an overdense spherical region of radius $R \approx \lambda \approx 10^4$ fm being left behind in thermal equilibrium in the hadron phase. This region, which probably represents the most important relic of the transition, will be subject to further subsequent diffusion.

As pointed out by Ignatius et al. [18], a number of conditions would need to be met if baryon number segregation is to have any significant effect on nucleosynthesis. One of these conditions (that the final baryon number density contrast should be larger than ~ 10) is certainly satisfied by the results from our present study. However, our results also indicate that the condition for the high density regions to contain most of the total baryon number is extremely difficult to satisfy unless turbulent diffusion might be operative. A third necessary condition requires that the mean separation scale l_n between two baryon number density peaks of the type computed here should be rather large. It would be necessary to have $l_n > 1 \text{ m} \approx 10^{-4} t_H$, where t_H is the horizon scale at the time of the transition. As mentioned in the Introduction, this is a fundamental quantity for the whole description of the phase transition, without which any conclusion about the role played by baryon number

inhomogeneities on the subsequent nucleosynthesis remains extremely unclear. Considerable efforts have been devoted to determining it (see Christiansen and Madsen [24] for a recent discussion) but the value of this scale is still uncertain and further developments need to be awaited.

The hydrodynamical scenario for baryon number segregation discussed here, could represent a promising starting point for studying the possible production of seed magnetic fields during the quark–hadron phase transition. Cheng and Olinto [25] pointed out that because of the different fractional electric charge carried by up and down quarks, charge separation could be produced together with the concentration of baryon number in the high temperature phase. In their paper, they focussed attention on the slow growth stage of the phase transition during which chemical equilibrium holds and the baryon number contrast can be estimated analytically. However, this same mechanism might be at work also during the final stages of the transition, for which the present calculations provide more precise quantitative estimates of the dynamical motions of charges and of their density.

Because of the much more extreme baryon number concentrations arising in the present context, the magnetic field could be several orders of magnitude larger than that discussed in [25] and might possibly reach the equipartition value. This requires further investigation and will be a focus of future work.

Acknowledgments

It is a pleasure to thank John C. Miller for his guiding comments, for suggesting the convenient finite difference expression (31) and for carefully reading this manuscript.

Appendix

In this Appendix, we briefly sketch some intermediate steps leading to equation (29), the relativistic diffusion equation for baryon number. Using the standard property of four-divergences mentioned in the text, equation (28) can be written as

$$bR^2 \left[(n_b)_{,t} + n_b \left(\frac{b_{,t}}{b} + \frac{2R_{,t}}{R} \right) \right] = -ab \left[R^2 q^\mu \left(\frac{a_{,\mu}}{a} + \frac{b_{,\mu}}{b} \right) + (R^2 q^\mu) \right]. \quad (36)$$

The T_1^0 component of the Einstein field equation provides the useful relation

$$\frac{b_{,t}}{b} = \frac{R_{,\mu t}}{R_{,\mu}} - \frac{a_{,\mu}}{aR_{,\mu}} - 4\pi GRabw_1 \approx \frac{R_{,\mu t}}{R_{,\mu}} - \frac{a_{,\mu}}{aR_{,\mu}} = \frac{a}{b\Gamma} u_{,\mu}, \quad (37)$$

where $G \ll 1$ is the gravitational constant and we drop the term containing it for the present purposes. Making use of the identity

$$\frac{b_{,\mu}}{b} = \frac{R_{,\mu\mu}}{b\Gamma} - \frac{\Gamma_{,\mu}}{b\Gamma}, \quad (38)$$

and of the definition (30), it is then possible to rewrite equation (36) in the final form (29).

References

- [1] E. Witten, Phys. Rev. D **30**, 272 (1984)
- [2] C. Alcock, G.M. Fuller and G.J. Mathews Ap. J. **320**, 439 (1987)
- [3] G.M. Fuller, G.J. Mathews and C. R. Alcock, Phys. Rev. D **37**, 1380 (1988)
- [4] H. Kurki-Suonio, Phys. Rev. D **37**, 2104 (1988)
- [5] C. Alcock, G.M. Fuller G.J. Mathews and B. Meyer, Nucl. Phys. A **498**, 301 (1989)
- [6] S. A. Bonometto and O. Pantano, Phys. Rep. **228** 175 (1993)
- [7] J. Ignatius, K. Kajantie, H. Kurki-Suonio and M. Laine, Phys. Rev. D **49**, 3854 (1994)
- [8] R. A. Malaney and G. J. Mathews, Phys. Rep. **229**, 145 (1993)
- [9] K. Jedamzik, G.M. Fuller, G.J. Mathews and T. Kajino Ap. J. **422**, 423 (1994)
- [10] J.H. Applegate, C.J. Hogan, Phys. Rev. D **31**, 3037 (1985)
- [11] L. Rezzolla and J. C. Miller Phys. Rev. D **53**, *in press* (1996)
- [12] L. Rezzolla and J. C. Miller, Class. Quantum Grav. **11**, 1815 (1994)
- [13] J. C. Miller and L. Rezzolla, Phys. Rev. D **51**, 4017 (1995)
- [14] L. Rezzolla, J.C. Miller and O. Pantano, Phys. Rev. D **52**, 3202 (1995)
- [15] A. Goyal, S. Pathak, V. K. Gupta and J. D. Anand Ap. J. **452**, 501 (1995)

- [16] J. C. Miller and O. Pantano, Phys. Rev. D **40**, 1789 (1989)
- [17] J. C. Miller and O. Pantano, Phys. Rev. D **42**, 3334 (1990)
- [18] J. Ignatius, K. Kajantie, H. Kurki-Suonio and M. Laine, Phys. Rev. D **49**, 3738 (1994)
- [19] H. Kurki-Suonio and M. Laine, Preprint HU-TFT-95-71 (1995)
- [20] K. Kajantie and H. Kurki-Suonio, Phys. Rev. D **34**, 1719 (1986)
- [21] K. Sumiyoshi, K. Kusaka, T. Kamio, T. Kajino, Phys. Let. B **225**, 10 (1989), K. Sumiyoshi, T. Kajino, C. R. Alcock and G.J. Mathews, Phys. Rev. D **42**, 3963 (1990)
- [22] D. Potter, *Computational Physics*, John Wiley and Sons, New York (1980)
- [23] E. S. Oran, J. P. Boris, *Numerical Simulation of Reactive Flow*, Elsevier, New York (1987)
- [24] M. B. Christiansen and J. Madsen, Phys. Rev. D **53**, 5446 (1996)
- [25] B. Cheng and A. Olinto, Phys. Rev. D **50**, 2421 (1994)